

Numerical investigation of a non-aqueous lithium-oxygen battery based on lithium superoxide as the discharge product

Peng Tan^a, Meng Ni^{a,b,*}, Zongping Shao^c, Bin Chen^a, Wei Kong^{a,d}

^a Department of Building and Real Estate, The Hong Kong Polytechnic University, Hung Hom, Kowloon, Hong Kong, China

^b Environmental Energy Research Group, Research Institute for Sustainable Urban Development (RISUD), The Hong Kong Polytechnic University, Hung Hom, Kowloon, Hong Kong, China

^c Department of Chemical Engineering, Curtin University, Perth, WA 6845, Australia

^d School of Energy and Power Engineering, Jiangsu University of Science and Technology, Jiangsu 212003, China

Abstract: It is reported lithium superoxide as the discharge product can largely decrease the charge voltage and enable a high round-trip efficiency of lithium-oxygen (Li-O₂) batteries. Here, we conduct a numerical investigation of the discharge behaviors of such batteries with LiO₂ as the discharge product. A mathematical model considering the mass transport and electrochemical reaction processes is first developed, which gives good agreement of the simulated discharge voltage with the experimental data. Then, with this model, the effects of electrode and electrolyte properties on the discharge performance are detailedly investigated. It is found that a thin cathode with a large porosity is favorable for a high specific capacity, and a high catalytic activity can lead to a high discharge voltage. For the cathode with different geometrical properties, it is found that the oxygen solubility and diffusivity have similar impacts on discharge capacities, but the oxygen solubility has a larger impact on energy densities. Besides, the limitations and further developments of the present model are also discussed. The results obtained from this work may give useful guidance for the discharge performance improvements of non-aqueous Li-O₂ batteries, and provide implications for other energy storage systems with solid product formation such as Na-O₂ batteries and Li-S batteries.

Keywords: Lithium-oxygen battery; Lithium superoxide; Cathode; Electrolyte; Numerical investigation.

* Corresponding author: Meng NI

Tel: 852-27664152; Fax: 852-27645131; Email: bsmengni@polyu.edu.hk

1. Introduction

Non-aqueous lithium-oxygen (Li-O₂) batteries are promising power sources in various applications, from portable electronic devices to electric vehicles [1], primarily due to the super-high energy density coming from two factors [2]: First, lithium has the theoretical capacity of 3,861 Ah kg⁻¹, corresponding to an energy density of ~11,680 Wh kg⁻¹ for a voltage of about 3.0 V. Second, the active component, oxygen, can be obtained from ambient air instead of occupying the mass and volume of the air electrode, increasing the energy density of the battery.

During discharge of a non-aqueous Li-O₂ battery, lithium metal is oxidized at the anode, producing electrons and lithium ions. At the cathode, oxygen is reduced and combined with electrons and lithium ions to form lithium peroxide (Li₂O₂). This oxygen reduction reaction (ORR) is summarized in Reaction I:



Since Li₂O₂ is insoluble in the non-aqueous electrolyte, it accumulates in the pores of the cathode with an increase in the capacity, which can eventually cover the triple-phase boundaries among oxygen, lithium ions, and electrons [3], terminating the discharge process and leading to a lower practical capacity [4]. During charge, the solid Li₂O₂ is electrochemically oxidized, producing electrons, lithium ions, and O₂. Due to the insulator nature of bulk Li₂O₂ [3], the charge overpotential is high, resulting in a low round-trip efficiency [5]. In addition, such a high potential can cause the decomposition of electrolytes and electrodes, forming irreversible side products passivating the active surfaces and leading to a limited cycle life [6]. To

solve these issues, tremendous efforts have been devoted, including searching for suitable electrolyte and electrode materials, developing effective catalysts, and designing proper cathode structures [7]. In the past decade, some breakthroughs have been achieved in lowering the charge voltage of non-aqueous Li-O₂ batteries. For instance, RuO₂ has been found to be an effective catalyst for the oxygen evolution reaction (OER) [8,9], resulting in a round-trip efficiency as high as around 80% [10]. Soluble redox mediators, which can facilitate the oxidation of solid Li₂O₂ in the charge process, have also been developed [11,12], enabling a charge voltage of less than 3.5 V and a long cycle life up to 900 times [13].

In addition to addressing the high charge voltage caused by Li₂O₂, investigations focused on the discharge product have also been carried out. One striking finding is that lithium superoxide (LiO₂), which was regarded as an intermediate product during discharge [14], can also exist in the final product. Yang *et al.* observed two voltage plateaus during charge, and Raman and magnetic measurements demonstrated that the lower plateau corresponded to a form of Li₂O₂ with superoxide-like properties [15]. With a large surface area activated carbon and an ether-based electrolyte, Zhai *et al.* identified two components in the discharge product, including an oxygen-rich component with superoxide-like character and a Li₂O₂ component, and the oxygen-rich domain is in the grain boundaries and outer parts of the product [16]. Xia *et al.* found that the physical and chemical properties of the Li₂O₂ depended on the discharge depth and overpotentials [17]. When the voltage decreases below 2.65 V in a deep discharge, the defective superoxide-structured phase with high conductivity is

formed on the rims of Li_2O_2 toroids. Although the formation of LiO_2 decreases the theoretical specific capacity of the battery as listed in **Table 1**, due to its higher electronic and ionic conductivities than those of Li_2O_2 [18], the charge voltage can be largely decreased and enable an improved round-trip efficiency. Hence, how to improve the ratio of LiO_2 in the discharge product attracts great interests recently. Curtiss *et al.* found that introducing small amounts of potassium into the activated carbon cathode material in the synthesis process could lead to a larger amount of LiO_2 in the discharge product [19]. Liu *et al.* reported that a cathode composed of ZnO nanoparticles anchored on vertically aligned carbon nanotubes could significantly suppress LiO_2 disproportionation, forming the composites of LiO_2 , Li_3O_4 and Li_2O_2 in nanometer size as the final discharge products [20]. Xiao *et al.* developed a cathode based on electro-deposited Pd nanoparticles on graphene [21]. Owing to the stronger binding energy between LiO_2 and the Pd surface, amorphous Li_2O_2 with higher ionic conductivity of Li^+ and O_2^{2-} was generated, resulting in the improved charge performance with the voltage as low as 3.08 V. With a cathode made of Ir nanoparticle-decorated reduced graphene oxide (Ir-rGO), Lu *et al.* achieved a Li- O_2 battery with pure LiO_2 as the product [22]. The crystalline LiO_2 was stable enough for the battery to be repeatedly charged and discharged with a low charge voltage of 3.2 V.

The further development of this novel technology involves insights into the multi-phase transport phenomena and the electrochemical processes during the battery operation. In parallel to experimental explorations, mathematical models play

important roles in understanding the coupled transport and electrochemical phenomena, predicting the battery performance, and optimizing the electrode structures [23,24]. For instance, Li and Faghri developed a two-dimensional model to study the mass transfer properties inside the cathode [25]. They found that most of the available pores deep in the cathode were not utilized, because Li_2O_2 accumulated at the oxygen inlet side blocked the oxygen transport pathway. To this end, a unique design of the cathode with a non-uniform porosity distribution was proposed to improve the discharge capacity and improved performance was experimentally verified [26]. Sahapatombut *et al.* used a micro-macro homogeneous model to study the influence of irreversible Li_2CO_3 formed from electrolyte solution degradation on battery performance [27]. The cycling simulation clearly showed a decrease of capacity retention with cycle numbers due to the pore blockage by Li_2CO_3 , which well explained the capacity degradation in experiments [28]. Hence, the combination of modeling and experimental investigations can effectively accelerate the development of non-aqueous Li-O₂ batteries.

Although there are plenty of modeling works and numerical investigations on non-aqueous Li-O₂ batteries with Li_2O_2 as the discharge product [29,30], no modeling study has been reported on the newly reported battery with LiO_2 as the discharge product. Due to the different reaction kinetics and different transport properties between Li_2O_2 and LiO_2 , there is a need to systematically investigate the behaviors of the LiO_2 -based Li-O₂ battery. To this end, we developed a mathematical model with macroscopic continuum approach to simulate the discharge behaviors of a

non-aqueous Li-O₂ battery based on LiO₂ as the product. After model validation with experimental data, the model was employed to investigate the effects of electrode and electrolyte properties on the discharge performance of the new battery. Finally, guidance for the electrode design and the electrolyte selection was also highlighted.

2. Model development

As schematically shown in **Fig. 1**, a non-aqueous Li-O₂ battery consists of a Li metal anode electrode, a microporous separator, and a porous cathode electrode saturated with a non-aqueous electrolyte. Through carefully selecting cathode materials (e.g., graphene-based), solid LiO₂ can be stabilized in the porous cathode as the main discharge product instead of forming other products (e.g., Li₂O₂, LiOH, and Li₂CO₃) [22]. Hence, the electrochemical reaction inside the cathode can be expressed as:



Since a battery system is complex with various mass transport and reaction processes, for simplicity, the following assumptions are made:

(1) The non-aqueous electrolyte of the battery, i.e., 1 M LiCF₃SO₃ in tetraethylene glycol dimethyl ether (TEGDME), is regarded as a binary solution.

(2) Only the formation of LiO₂ in the porous cathode is considered (**Fig. S1**).

The parasitic reactions and the decomposition of electrolyte and electrode are neglected [22].

(3) The pores within the cathode are fully occupied by the liquid electrolyte

initially. The movement of the electrolyte due to the volume change of solid phases (e.g., lithium anode consumption, LiO_2 formation) [31] and the solvent evaporation is neglected [32].

- (4) The mass convection inside the battery is negligible [33]. The Knudsen diffusion effect is not considered [29,30,34].
- (5) At the present low current densities (e.g., 0.1 mA cm^{-2}), the temperature changes are found to be negligible [25,35], so that the thermal effect is not considered.

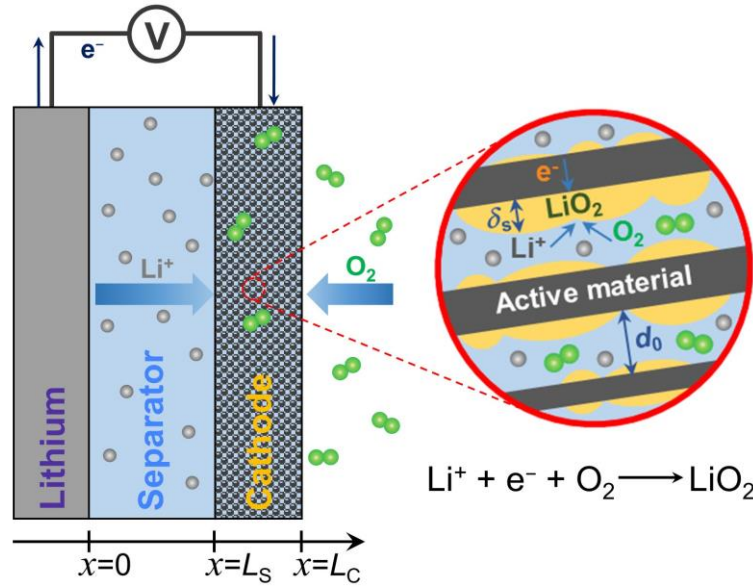


Fig. 1 Schematic diagram of a non-aqueous Li- O_2 battery during discharge. The inset demonstrates the reaction occurs inside the graphene-based cathode with the formation of LiO_2 as the product.

2.1 Governing equations

A one-dimensional transient model based on the macroscopic approach is developed according to the previous work [29]. In the porous cathode, the conservation of species i (Li^+ and O_2) can be written as:

$$\frac{\partial(\varepsilon c_i)}{\partial t} = -\nabla \cdot \mathbf{N}_i + S_i \quad (1)$$

where c_i is the bulk concentration of species i in the electrolyte, which is averaged over the volume of the electrolyte in the pores. ε is the volume fraction of void space that is filled with liquid electrolyte and changes with the formation of the solid product. \mathbf{N}_i is the molar flux of species i in the electrolyte, and S_i is the generation or consumption rates of species i due to the electrochemical reaction. By neglecting the convection transport, the molar flux of Li^+ and O_2 can be defined as:

$$\mathbf{N}_{\text{Li}^+} = -D_{\text{Li}^+}^{\text{eff}} \nabla c_{\text{Li}^+} + \frac{\mathbf{i}_1 t_+}{F} \quad (2a)$$

$$\mathbf{N}_{\text{O}_2} = -D_{\text{O}_2}^{\text{eff}} \nabla c_{\text{O}_2} \quad (2b)$$

where $D_{\text{Li}^+}^{\text{eff}}$ and $D_{\text{O}_2}^{\text{eff}}$ are the effective diffusion coefficient of Li^+ and O_2 , respectively. t_+ is the transference number of Li^+ , F is Faraday constant (96485 C mol⁻¹), \mathbf{i}_1 is the current density in the liquid phase (electrolyte) and can be obtained through treating the non-aqueous electrolyte as a binary concentrated solution as:

$$\mathbf{i}_1 = -\kappa^{\text{eff}} \nabla \phi_1 - \frac{2RT\kappa^{\text{eff}}}{F} (t_+ - 1) \left(1 + \frac{\partial \ln f_{\pm}}{\partial \ln c_{\text{Li}^+}}\right) \nabla \ln c_{\text{Li}^+} \quad (3)$$

where κ^{eff} is the effective ionic conductivity, ϕ_1 is the potential in the electrolyte, R is the universal gas constant (8.3143 J mol⁻¹ K⁻¹), T is the temperature in Kelvin, f_{\pm} is the activity coefficient of lithium salt.

In the cathode, the current density in the solid phase \mathbf{i}_s is governed by Ohm's law through the electric potential ϕ_s as:

$$\mathbf{i}_s = -\sigma^{\text{eff}} \nabla \phi_s \quad (4)$$

where σ^{eff} is the effective electronic conductivity of the electrode.

The effective parameters $D_{\text{Li}^+}^{\text{eff}}$, $D_{\text{O}_2}^{\text{eff}}$, κ^{eff} , and σ^{eff} in the above equations are usually dependent on the tortuosity of respective phase in the porous cathode. These parameters for the porous cathode are corrected to account for the porosity effect using Bruggeman correlation as:

$$D_{\text{Li}^+}^{\text{eff}} = \varepsilon^\alpha D_{\text{Li}^+} \quad (5a)$$

$$D_{\text{O}_2, \text{e}}^{\text{eff}} = \varepsilon^\alpha D_{\text{O}_2, \text{e}} \quad (5b)$$

$$\kappa^{\text{eff}} = \varepsilon^\alpha \kappa \quad (5c)$$

$$\sigma^{\text{eff}} = (1 - \varepsilon)^\alpha \sigma \quad (5d)$$

where α is the Bruggeman coefficient and the typical value of 1.5 is used. D_{Li^+} , D_{O_2} , κ , and σ are the diffusion coefficient of Li^+ and O_2 in the electrolyte, the ionic conductivity of the electrolyte, and the electrical conductivity of the electrode, respectively.

For the macroscopic model, the charges are conserved between the liquid and solid phases and can be expressed through the divergence of the current density as:

$$\nabla \cdot \mathbf{i}_l + \nabla \cdot \mathbf{i}_s = 0 \quad (6)$$

and the transfer current density at electrolyte/electrode interface can be calculated by:

$$\nabla \cdot \mathbf{i}_l = aj \quad (7)$$

where a is the surface area per unit volume of the electrode, and j is the transfer current density. Since only one electrochemical reaction (Reaction II) occurs inside the cathode, the reaction rate of species i is given by Faraday's law as:

$$S_i = -\frac{as_i}{F} j_c \quad (8)$$

where s_i is the corresponding stoichiometric coefficient of species i .

For the electrochemical reaction at the lithium anode, the local transfer current density between anode and electrolyte interface (j_a) can be given by the general Butler-Volmer equation as:

$$j_a = i_0 \left\{ \exp \left[\frac{(1-\beta)F}{RT} \eta_a \right] - \exp \left(\frac{-\beta F}{RT} \eta_a \right) \right\} \quad (9)$$

where i_0 is the exchange current density at the anode, and β is the symmetry factor equal to 0.5, η_a is the overpotential at the anode and is given by:

$$\eta_a = \phi_M - \phi_l - E_a^0 \quad (10)$$

in which ϕ_M is the potential of the metallic lithium and is chosen to be zero, E_a^0 is the theoretical equilibrium potential for the lithium dissolution reaction.

For the electrochemical reaction at the cathode, the local transfer current density j_c depends on both concentration of Li^+ and O_2 and the concentration of LiO_2 (Reaction II):

$$j_c = F \left\{ k_a (c_{\text{LiO}_2,s}) \exp \left[\frac{(1-\beta)F}{RT} \eta_c \right] - k_c (c_{\text{Li}^+,s})(c_{\text{O}_2,s}) \exp \left(\frac{-\beta F}{RT} \eta_c \right) \right\} \quad (11)$$

where $c_{i,s}$ is the molar concentration of species i at the surface of the cathode, k_a and k_c are the anodic and cathodic rate constant, respectively. η_c is the overpotential at the cathode and is given by:

$$\eta_c = \phi_s - \phi_l - E_c^0 - \Delta\phi_{\text{LiO}_2} \quad (12)$$

in which E_c^0 is the theoretical equilibrium potential for the oxygen reduction reaction and $\Delta\phi_{\text{LiO}_2}$ is the voltage loss through the solid LiO_2 deposition. From the reported works in which LiO_2 is the final discharge product, catalyst-decorated graphene is used as the electrode material [21,22]. At the initial capacity of 1000 mAh

g^{-1} , the product with a needle- or rod-like morphology was observed, but connected to each other forming a deposition layer with the capacity increasing [22]. For simplicity, we treat the LiO_2 deposition as a film covering the cathode surface [23,24,36]. Hence, the voltage loss can be expressed as [36]:

$$\Delta\phi_{\text{LiO}_2} = j_c R_s \delta_s \quad (13)$$

where R_s is the electrical resistivity across LiO_2 film, δ_s is the deposition film thickness and could be obtained using:

$$\delta_s = \frac{d_0 \varepsilon_s}{2\varepsilon_0} \quad (14)$$

where d_0 is the distance between two graphene plat, ε_s is the volume fraction of the solid product, and ε_0 is the initial porosity.

The solid LiO_2 precipitates in the porous cathode during discharge, covering the surface and occupying the void volume. The volume change due to the accumulation of solid LiO_2 can be easily obtained as:

$$\frac{\partial \varepsilon_s}{\partial t} = a j_c \frac{M_{\text{LiO}_2}}{F \rho_{\text{LiO}_2}} \quad (15)$$

where M_{LiO_2} and ρ_{LiO_2} are the molecular weight and density of LiO_2 , respectively.

The effective local surface area per unit volume of the air electrode due to LiO_2 coverage is commonly approximated by a geometric relation as [29]:

$$\frac{a}{a_0} = 1 - \left(\frac{\varepsilon_s}{\varepsilon_0} \right)^p \quad (16)$$

where a_0 is the initial specific surface area, p is a geometrical factor indicating the morphology of the solid product that covers the active area. Small values of p indicate the flat, plate-like precipitate. Here, the value of 0.5 has been selected in this work.

2.2 Boundary conditions

From **Fig. 1**, the computational domain includes the anode/separator interface, the separator, the separator/cathode interface, the cathode, and the cathode/oxygen interface (from $x=0$ to $x=L_C$), as listed in **Table S1**. The boundary conditions are thus defined accordingly as follows [29]:

At the anode/separator interface ($x=0$), lithium metal is electro-oxidized to compensate the consumption of Li^+ and electric migration in the electrolyte, which is expressed as:

$$-\frac{\partial N_{\text{Li}^+}}{\partial x} = (1 + t_+) \frac{i_{\text{app}}}{F} \quad (17)$$

where i_{app} is the applied discharge current density. The oxygen concentration (c_{O_2}) is set to be zero.

At the separator/cathode interface ($x=L_S$), the continuous boundary conditions are specified for the fluxes of all species. The current density in the solid phase becomes zero, and the current density in the electrolyte equals to the applied discharge current density, which can be expressed as:

$$i_s = 0 \quad (18)$$

$$i_l = i_{\text{app}} \quad (19)$$

At the cathode/oxygen interface ($x=L_C$), the oxygen concentration is constant with the saturated value in 1 M $\text{LiCF}_3\text{SO}_3/\text{TEGDME}$ due to the continuous feeding of gaseous oxygen. On the contrary of the separator/cathode interface, the current density in the solid phase equals to the discharge current density, whereas the current density in the electrolyte becomes zero.

The voltage of the battery is calculated by the difference between the electrode potential at cathode current collector and the electrolyte potential at the anode side as:

$$E = \phi_s(x = L_c) - \phi_l(x = 0) \quad (20)$$

2.3 Numerical conditions

Initial conditions are specified for the Li^+ and O_2 concentrations, the porosity, the specific surface area, and the separator and cathode thicknesses. These values applied in the model are summarized in **Table 2**. In many reported modeling works, a cathode with the thickness of 100–800 μm was applied [36]. Due to the low transport coefficients of Li^+ and O_2 in non-aqueous electrolytes, a non-uniform distribution of species was found, resulting in the low utilization of the porous cathode [25]. To improve the transport kinetics and the utilization of active materials, the cathode in experiments is generally composed of a thin active layer ($<10 \mu\text{m}$) on a gas diffusion layer/current collector (100 μm , e.g., carbon paper, nickel foam) [37], including the one made of Ir-rGO on a carbon paper (TGP-H-030, Toray) in the LiO_2 -based battery [22]. Hence, the term “cathode” in this work refers to the active layer that participates in the reaction, and a small value of thickness (i.e., 5 μm) was therefore chosen in calculation to validate the model. Before discharge, the oxygen was assumed to dissolve in the electrolyte with the saturated concentration. The concentration of each species was assumed to be uniform at all locations inside the computational domain and equal to their initial concentration. Compared with Reaction I, The open circuit voltage ($E_c^0 - E_a^0$) for Reaction II has been few discussed in the literature [38]. Padbury and Zhang reported a value of 3.0 V [39], and Fan *et al.* calculated a value of

2.98 V under the condition of 300 K and 1 atm (O_2) [20]. Here we still choose the value of 2.96 V and assume it is independent of the concentration of oxygen or lithium ions for simplicity. For a demonstrative study of kinetics, the rate constants of k_a and k_c are preliminarily adjusted, respectively.

The conservation equations and the boundary conditions described above were discretized using a finite element method. The different transport equations and the electrochemical reactions were solved as time dependent. The solution was considered to be converged when the relative tolerance was less than 10^{-4} . The one dimensional coupled partial differential equations described above are discretized by quadratic elements, forming an algebraic equation system using a finite element method. The algebraic equation system is solved by the MUMPS method [45] with its non-linearity taken care by Newton method. In the time stepping, the backward differentiation formula (BDF) method [46] is employed to discretize the simulated time span with the maximum time step of 0.1 second. In each time step, the voltage was calculated according to Eq. 18 and compared with a cut-off voltage of 2.2 V. To compare the results with experimental data, the calculation was based on the discharge current density of 100 mA g^{-1} , and the discharge capacity was converted to the specific value (mAh g^{-1}) accordingly [47].

3. Numerical Results

3.1 Model validation

The simulated voltage curve of the Li- O_2 battery based on LiO_2 is shown in **Fig. 2**, and compared with the experimental data [22]. At a capacity limit of 1000 mAh g^{-1} ,

crystalline LiO_2 was reported to be the discharge product through various characterization techniques and is stable enough for repeated discharge and charge cycles (**Fig. S1**). The discharge voltage from our modeling is around 2.70 V, which shows good agreement with experimental results as indicated in **Fig. 2a**. To further verify this model, a deep discharge with a cut-off voltage of 2.2 V is set. From **Fig. 2b**, similar discharge voltage curves as well as discharge capacities can be found. The voltage difference after the capacity of 6000 mAh g^{-1} may come from the side reactions occurred in experiments: when the battery was run to a deep discharge of 2.2 V, the presence of LiO_2 , Li_2O_2 and LiOH was identified; while in our simulation, LiO_2 was considered as the only product without any side reactions. Overall, the model results and experimental data show good agreement, validating the present model for further numerical analyses. It is known that side reactions, including the formation of Li_2O_2 and the decomposition of electrolyte and electrode, are detrimental to the battery performance (e.g., high charge voltage, low energy efficiency, and short cycle life) and should be avoided in the real application. Hence, with the present model, we will detailedly investigate the effects of different electrode and electrolyte properties on the discharge behaviors of ideal LiO_2 -based batteries in the following part. The incorporation of side reactions in the modeling work will be further discussed in the next section.

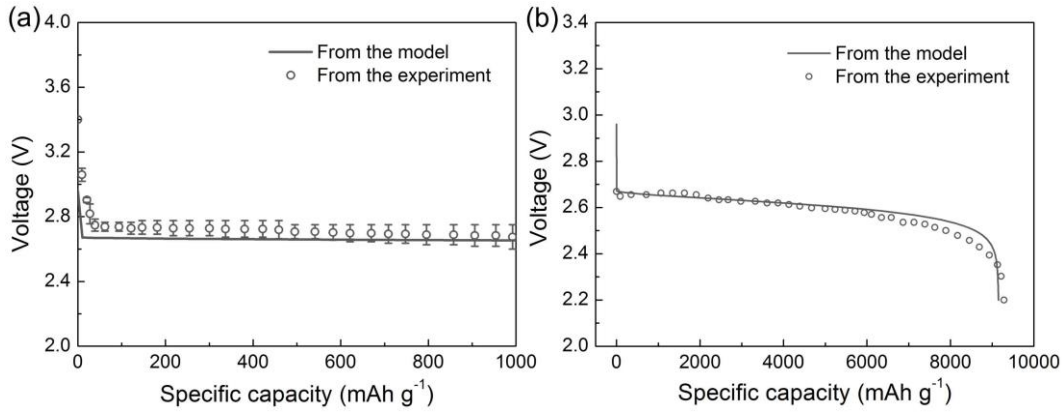


Fig. 2 Comparisons between simulated discharge curves and experimental data from Ref. [22]: (a) with a capacity limit of $1,000 \text{ mA h g}^{-1}$, the error bar shows the variation of discharge voltages during cycling; (b) deep discharge to a cut-off voltage of 2.2 V.

3.2 Cathode design

The cathode plays a crucial role in the discharge performance of Li-O₂ batteries, and the effects of different factors have been experimentally and numerically investigated [48]. Based on the product of LiO₂, we study the influence of cathode design on the discharge behaviors in this section. First, the geometrical factors, including the thickness and porosity, are investigated. It is worth noting that for a given cathode material (e.g., Ir-rGO), the change of thickness or porosity will inevitably alter the loading of active material. To this end, different from previous modeling works that use the current density based on the surface area (mA cm^{-2}) [29,41], we use the current density based on the mass (100 mA g^{-1}) to compensate for the changes of loading. In addition, as different cathode materials have different activities [21], the corresponding effects on the discharge performance are also discussed.

3.2.1 Effect of geometry

As indicated in Eq. 2, the molar flux of Li^+ and O_2 is closely related to the cathode thickness, which will affect the electrochemical reaction. The discharge voltage curves of the battery with different cathode thicknesses are shown in **Fig. 3a**. When the thickness increases from 5 μm to 10 μm and even 20 μm , the capacity exhibits a slight decrease to 8915 mAh g^{-1} and 8323 mAh g^{-1} , respectively. When further increasing the thickness to 50 μm , the specific capacity shows a large decrease to 6150 mAh g^{-1} (**Fig. 3b**), as well as the voltage plateau. Due to the formation of solid LiO_2 , both the oxygen concentration and the porosity along the thickness of the cathode changes with the discharge state (**Fig. S2**). To make comparisons of the oxygen concentration and the pore volume utilization in the cathodes with different thicknesses, we present the oxygen concentration and the porosity profiles at the end of the discharge stage. From **Fig. 3c**, it is found that the dimensionless depth for oxygen penetration decreases with increasing thickness, indicating a high oxygen transport resistance. As a result, the utilization of the porous cathode decreases with thickness as demonstrated in **Fig. 3d**. Hence, a thin cathode (or active layer) is favorable for a higher specific capacity [29,41]. However, a decrease in the thickness means that the loading of the active material is also decreased, which may lead to a low practical capacity (mAh) [49], as shown in **Fig. 3b**. In the present LiO_2 -based battery, the existence of LiO_2 without side products was achieved in a capacity-limited discharge (1000 mAh g^{-1}) [22], meaning that a high loading is required if deliver a large practical capacity, which may increase the cathode thickness.

Hence, a careful design of the cathode thickness is needed with considering the trade-off between the specific capacity and the practical capacity.

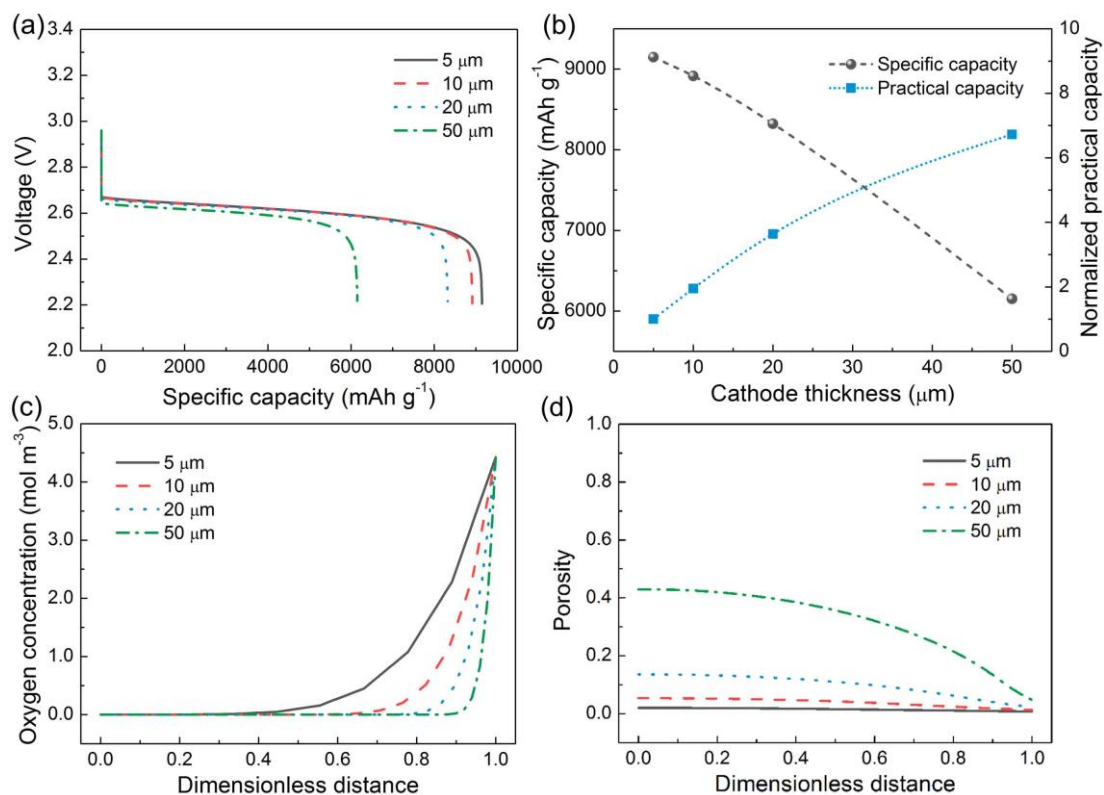


Fig. 3 Effect of cathode thickness on the discharge performance: (a) discharge voltage curves; (b) specific and practical capacities at different cathode thicknesses, the practical capacity is normalized using the capacity at the thickness of 5 μm; (c) oxygen concentration at the end of discharge; and (d) porosity profile at the end of discharge.

The discharge voltage curves at different porosities are shown in **Fig. 4a**. With a decrease of porosity, both the specific capacity and the voltage plateau decrease. As shown in **Fig. 4b**, a decrease of porosity from 0.94 to 0.40 dramatically reduces the capacity from 9150 mAh g⁻¹ to only 320 mAh g⁻¹. Similar results have also been reported by Sahapatombut *et al.* for Li₂O₂ as the product [29]. Even considering the

practical capacity, it still decreases with a decrease in the porosity (**Fig. 4b**). This may be attributed to the limited void space for the solid product storage and the high transport resistant at a low porosity, as indicated in Eq. 1 and Eq. 5, respectively. From **Fig. 4c**, at the same distance, the oxygen concentration for the cathode with a low porosity is higher than that with a high porosity. This may be caused by the low utilization of the pore volume at the end of discharge, remaining spaces for oxygen diffusion, as clearly demonstrated in **Fig. 4d**. Hence, to obtain a high discharge specific capacity, a large porosity is crucial for species transport and solid product accumulation. It is noting that previous works indicated that the pore size has a significant role in the discharge performance [48]. Even for a cathode with the same porosity, the pore size distribution can be different and result in different capacities. An insightful investigation with considering the pore size distribution will be conducted in the near future.

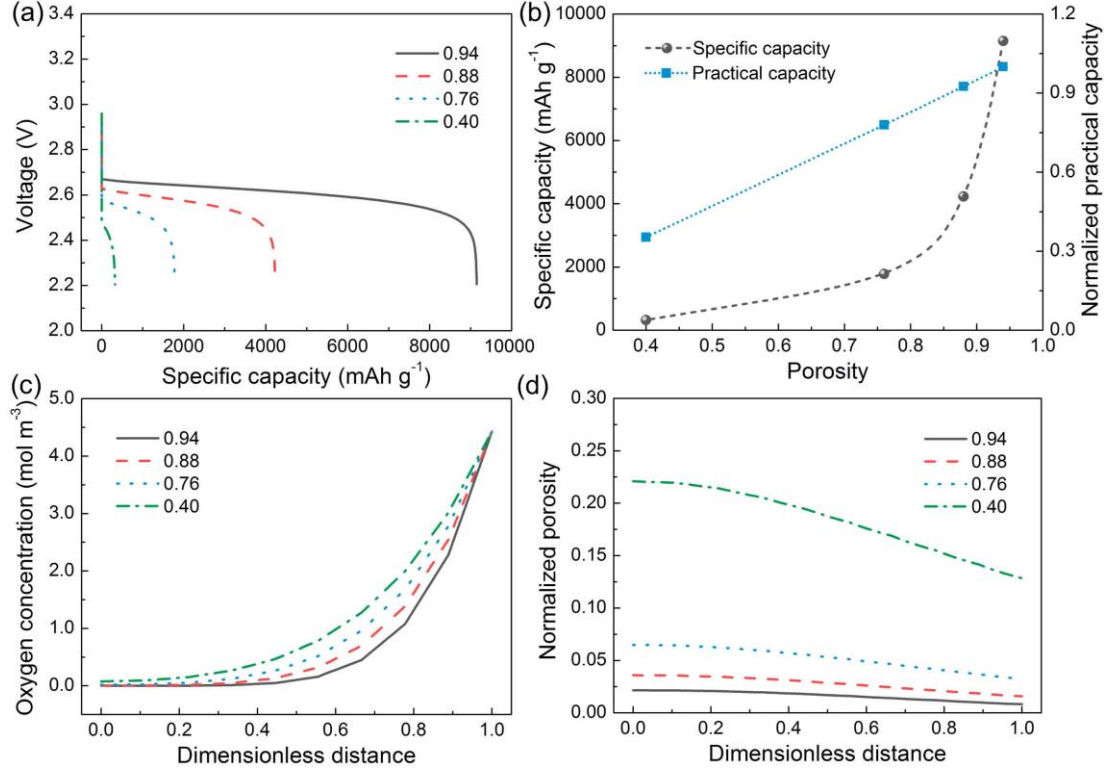


Fig. 4 Effect of cathode porosity on the discharge performance: (a) discharge voltage curves; (b) specific and practical capacities at different cathode thicknesses, the practical capacity is normalized using the capacity at the porosity of 0.94; (c) oxygen concentration at the end of discharge; and (d) normalized porosity profile at the end of discharge.

3.2.2 Effect of reaction activity

To investigate the effect of catalytic activity of the cathode on the discharge performance, we change the cathodic rate constant (k_c) with the ratio from 0.1 (1.4×10^{-16}) to 10 (1.4×10^{-14}). The discharge voltage curves at different rates are shown in **Fig. 5a**. At the cut-off voltage of 2.2 V, it is interesting to find that the discharge voltage clearly increases with an increase in the reaction rate, as summarized in **Fig. 5b**, whereas the capacity almost remains the same. This finding is different from the previous studies on non-aqueous Li-O₂ batteries with Li₂O₂ as the

product, as both specific capacity and discharge voltage have been improved through various kinds of catalysts [50]. However, the addition of some catalysts (e.g., RuO_2) increases the discharge voltage due to the improved oxygen reduction activities but decreases the specific capacity [51]. A possible reason for these different results could be the changes of the solid product morphology caused by the activity changes. If the product morphology changes from the film-like to particle-like, an improved utilization of the pore volumes can be achieved, resulting in an increased capacity [52]. In our numerical investigation, the morphology of the solid product that covers the active area is described through a geometrical factor p (Eq. 15), and a film-like LiO_2 morphology is assumed in various catalytic activities, which would lead to the unchanged specific capacity. If we assume the product morphology changes with reaction rate, e.g., at the low reaction rate a needle-like product is formed, while at the high rate a plate-like product is formed, the discharge capacity will be changed with the reaction activity (**Fig. S3**). It can be expected that with an in-depth understanding in the LiO_2 morphology evolution process, a more precise model to describe the discharge behaviors under different reaction activities can be developed.

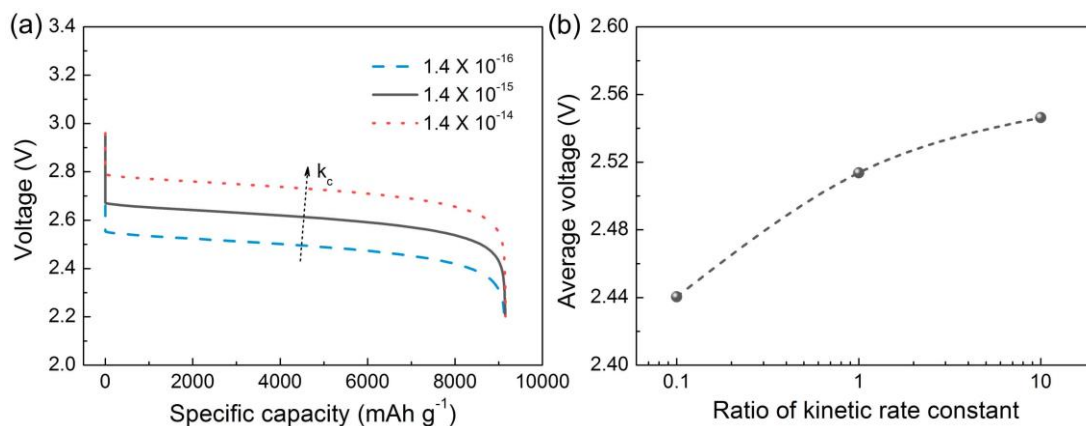


Fig. 5 Effect of reaction activity on the discharge performance: (a) discharge voltage

curves; (b) average discharge voltages at different reaction rates.

3.3 Electrolyte selection

An ideal non-aqueous electrolyte used in Li-O₂ batteries should have good chemical and electrochemical stability, high ionic conductivity, high boiling point, and high oxygen solubility and diffusivity [53]. For the formation of Li₂O₂, Bruce *et al.* proposed two different mechanisms: the solution mechanism and the surface mechanism, which are governed by the competition between the LiO₂ solubility and the adsorption free energy of LiO₂ on the cathode surface, respectively [54]. For the battery with LiO₂ as the product, the synergetic effect between the electrolyte and the cathode that can eventually stabilize LiO₂ is crucial [21,22]. Here, we do not consider the intrinsic properties of electrolytes (e.g. donor number, DN) [55], but focus on the effects of transport properties on the discharge performance in this section. Since Li⁺ concentration is three orders of magnitude higher than that of oxygen (**Table 2**), the oxygen transport is therefore regarded as one limiting factor for the discharge performance [39]. Hence, we consider the effects of oxygen solubility and diffusivity on different types of cathodes (pristine: L=5 μm, ε₀=0.94; thick: L=20 μm, ε₀=0.94; and compact: L=5 μm, ε₀=0.76). Although the influence of different electrolytes with various transport properties has been numerically investigated [56], the key property for the discharge performance was not identified. Here we assume the oxygen solubility and diffusivity are independent so that their importance on the discharge capacity and energy density can be compared and determined.

3.3.1 Effect of oxygen solubility

To investigate the effect of oxygen solubility on the discharge performance, we change the oxygen solubility with the ratio from 0.1 to 10, and the results are shown in **Fig. 6**. For the pristine cathode, when the ratio of oxygen solubility changes from 0.1 to 1.0, the discharge voltage plateau increases from 2.55 V to 2.67 V, and the capacity increases from 8568 mAh g⁻¹ to 9150 mAh g⁻¹ (an increase of 6.8%). The improvement in the voltage plateau comes from the improved reaction kinetics due to the increased oxygen concentration, as indicated in Eq. 11, which meanwhile produces more product and results in a higher capacity. When further increasing the ratio of oxygen solubility to 10, as shown in **Fig. 6a1**, although the voltage plateau keeps increasing, the capacity increases slightly. This may be attributed to the limited pore volume for solid product accumulation, as demonstrated in **Fig. 6a3**. At the ratio of 1.0, the cathode pore volumes have almost been utilized, leaving no spaces for further capacity improvement. Similar results can be found in the compact cathode as shown in **Fig. 6c**. While for the thick cathode, as shown in **Fig. 6b1**, both the discharge voltage plateau and the capacity substantially increases with the oxygen solubility. Because the oxygen transport route in the thick cathode is long, increasing the oxygen solubility can increase the overall oxygen concentration, and thus improves the utilization of the pore volume (**Fig. 6b3**). Hence, increasing the oxygen solubility can increase both the voltage plateau and the capacity, and the improvements are more apparent in a thick cathode with a high porosity.

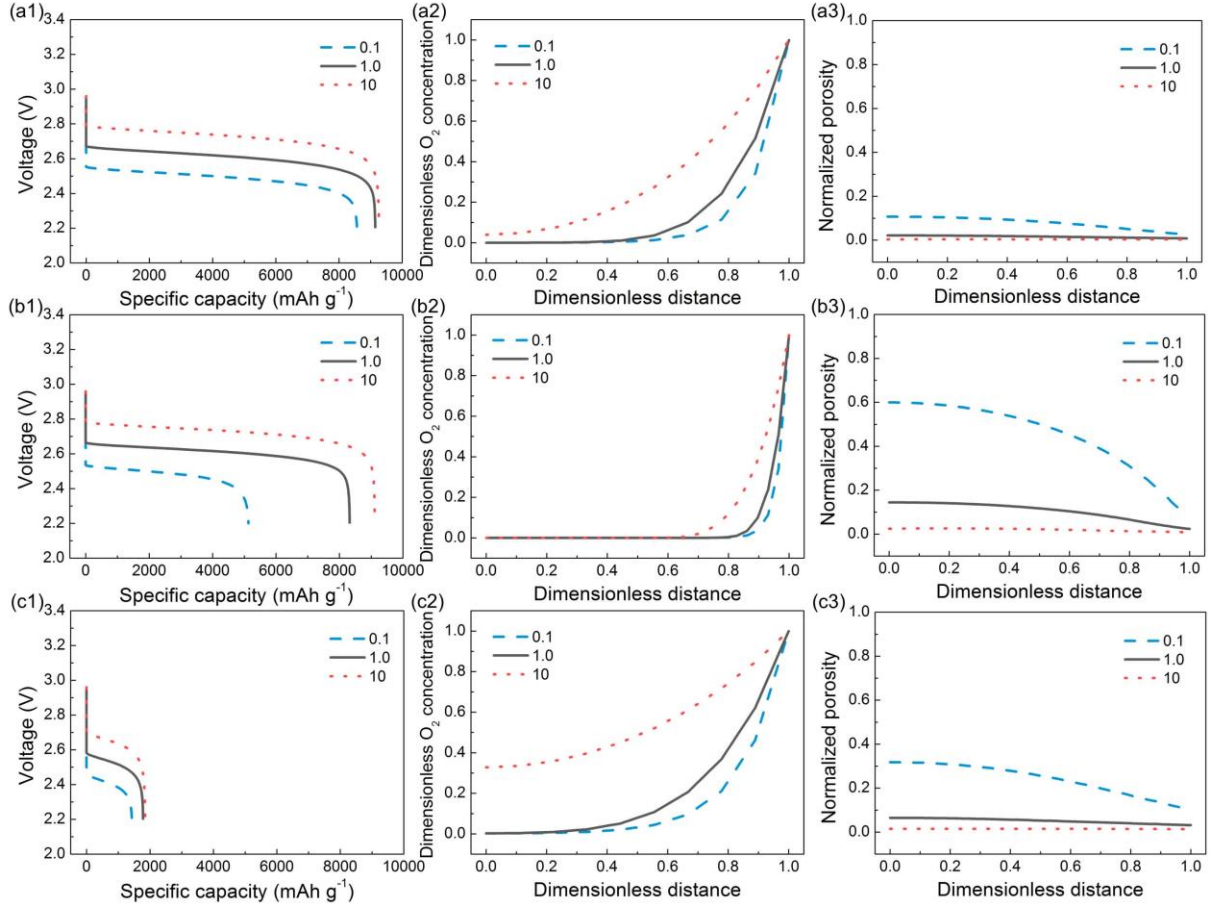


Fig. 6 Effect of oxygen solubility on the battery with (a) pristine cathode ($L=5\ \mu\text{m}$, $\varepsilon_0=0.94$), (b) thick cathode ($L=20\ \mu\text{m}$, $\varepsilon_0=0.94$), and (c) compact cathode ($L=5\ \mu\text{m}$, $\varepsilon_0=0.76$): (1) discharge voltage curves; (2) dimensionless oxygen concentration at the end of discharge; (3) normalized porosity profile at the end of discharge.

3.3.2 Effect of oxygen diffusivity

To investigate the effect of oxygen diffusivity on the discharge performance, similarly, we change the ratio from 0.1 to 10, and the results are shown in **Fig. 7**. For the pristine cathode (**Fig. 7a**), the capacity increases with the increasing ratio of oxygen diffusivity, which comes from the enhanced transport of oxygen to the reaction sites as indicated in Eq. 2, increasing the penetration depth (**Fig. 7a2**). However, different from the situation in changing oxygen solubility, the discharge

voltage changes slightly since the reaction kinetics is not directly correlated with the oxygen diffusivity (Eq. 11). Similar phenomena can be observed in the thick and the compact cathodes, as shown in **Fig. 7b** and **7c**, respectively. Therefore, increasing the oxygen diffusivity can mainly increase the discharge capacity.

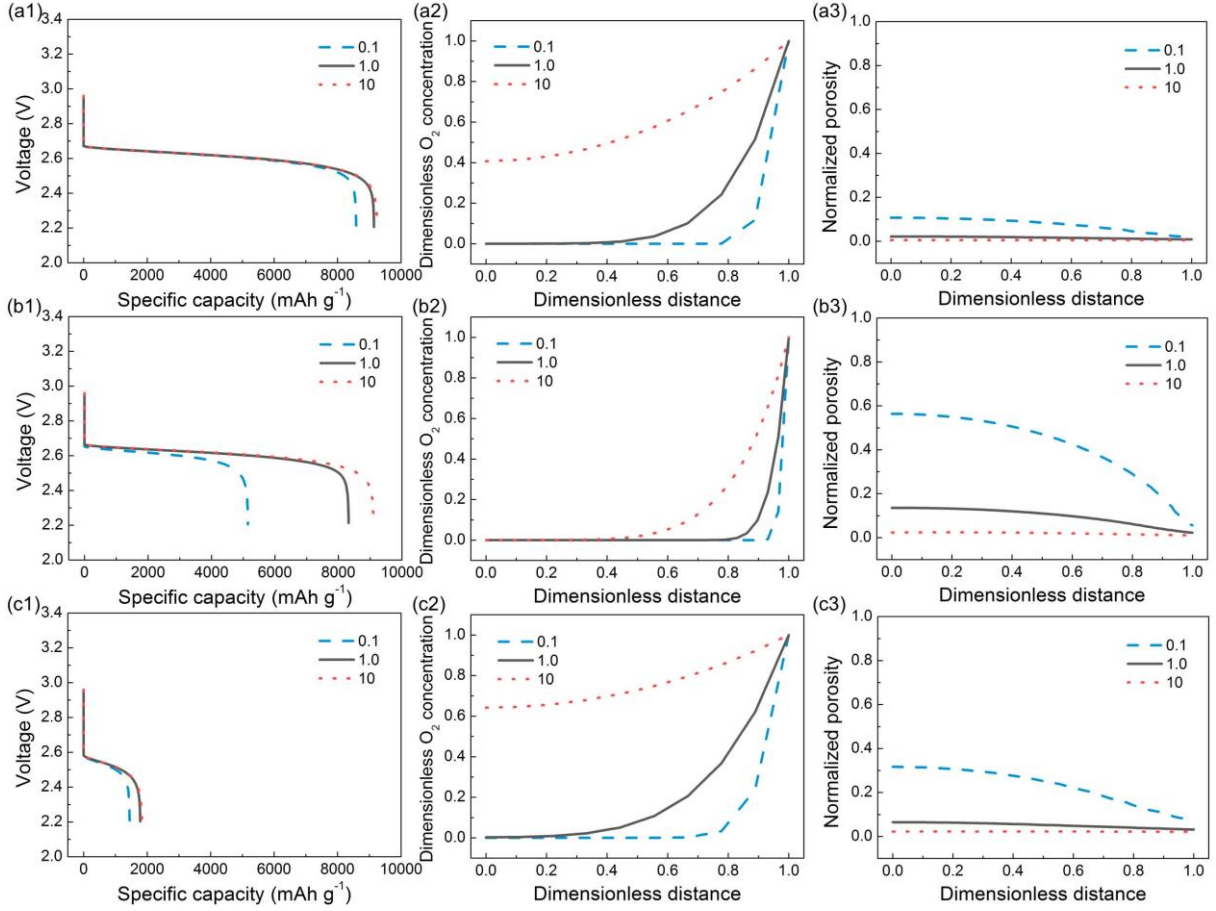


Fig. 7 Effect of oxygen diffusivity on the battery with (a) pristine cathode ($L=5\ \mu\text{m}$, $\varepsilon_0=0.94$), (b) thick cathode ($L=20\ \mu\text{m}$, $\varepsilon_0=0.94$), and (c) compact cathode ($L=5\ \mu\text{m}$, $\varepsilon_0=0.76$): (1) discharge voltage curves; (2) dimensionless oxygen concentration at the end of discharge; (3) normalized porosity profile at the end of discharge.

3.3.3 Electrolyte design

Based on the above results, the effects of oxygen solubility and diffusivity on the discharge performance can be compared. First, the discharge capacities of three kinds

of cathodes (pristine, thick, and compact) are normalized with the capacities obtained at the initial oxygen solubility and diffusivity (ratio equals to 1.0), and the results are shown in **Fig. 8a**. For pristine and thick cathodes, it is found that the oxygen solubility and diffusivity have almost the same impacts on the discharge capacity. Even so, the intrinsic reasons may be different: a higher oxygen solubility gives a larger initial value of dissolved oxygen in the electrolyte and leads to an enhanced reaction kinetics; while a higher oxygen diffusivity means a better transport kinetics so that the oxygen can penetrate faster and deeper into the cathode. This can be clearly observed in the thick cathode: when the ratios increase to 10, although in both case the resultant capacities are almost the same, a higher oxygen diffusivity leads to a larger penetration depth (**Fig. 7b2**). As a result, the oxygen solubility shows a little larger impact on the discharge capacity than that of the oxygen diffusivity when the cathode becomes compact, since the lower porosity results in a higher oxygen transport resistance as indicated in Eq. 5. To account for the influences on the discharge voltage, the specific energy densities are also compared using the similar normalization method. As shown in **Fig. 8b**, three kinds of cathodes demonstrate the same trend that the oxygen solubility has a larger impact than that of the oxygen diffusivity, which is mainly attributed to the improved reaction kinetics (Eq. 11). Hence, a high oxygen solubility is more favorable for achieving a larger discharge capacity and energy density.

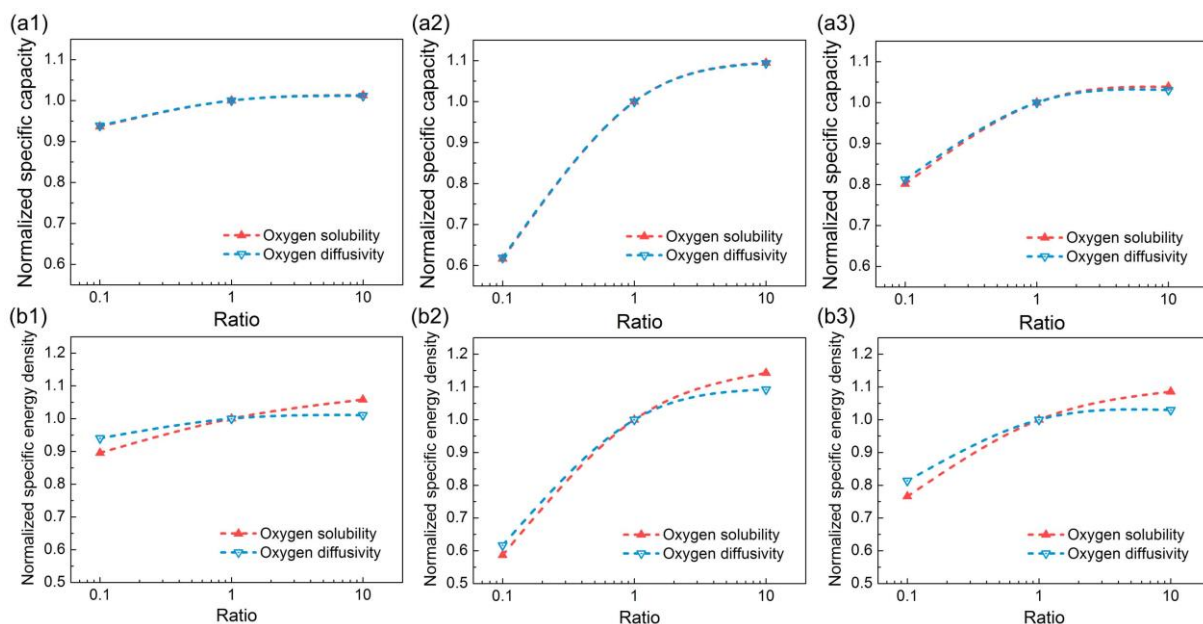


Fig. 8 Comparison of normalized (a) specific capacity and (b) energy density of the battery at different ratios with: (1) pristine cathode; (2) thick cathode (large thickness); (3) compact cathode (low porosity).

Generally, two kinds of non-aqueous solvents with different properties (**Table S2**) have been widely used in Li-O₂ batteries, including TEGDME and dimethyl sulfoxide (DMSO), and various kinds of lithium salts (e.g., LiNO₃, LiBF₄, LiClO₄, LiCF₃SO₃) have been tried, resulting in different transport properties (**Fig. S4**) [57]. It is found that in high DN solvents (i.e., DMSO), oxygen diffusivity is largely independent of salt concentration, anion choice, and oxygen partial pressure [58]. While in low DN solvents (i.e., TEGDME), oxygen diffusivity is influenced by salt concentration and anion choice. Oxygen solubility in electrolytes is influenced by both electrostatics and dispersion effects from dissociated ions, and large anions (i.e., TFSI⁻) can lead to higher oxygen concentrations than those of smaller anions (i.e., BF₄⁻) in the same solvent. It is worth noting that the lithium salt concentration is usually 1.0 M so that oxygen becomes the limiting reactant of mass transport due to the low dissolved O₂

concentrations. If an electrolyte with low salt concentrations is used, Li^+ mobility is equally critical to the battery operation, and Li^+ diffusion may also become the limiting factor and should also be carefully considered.

4. Discussion

From the numerical results, we have obtained implications for the cathode and electrolyte design for LiO_2 -based batteries. In this section, we discuss the further development of the present model for insightful investigations.

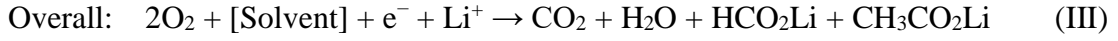
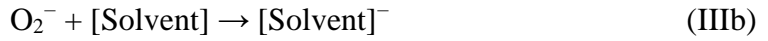
4.1 Side reactions

One key assumption in the present model is the formation of LiO_2 as the only product (Reaction II), which is based on the experimental observations [22]. However, side products like Li_2O_2 and LiOH could also be identified at a deep discharge. Although tremendous efforts should be made in suppressing and avoiding side reactions for practical application, understanding their effects on the battery performance is essential in the current stage.

The main side reactions can be divided into two types: i) the formation of Li_2O_2 and ii) the decomposition of the electrolyte solvent (i.e., TEGDME) due to the appearance of superoxide radical anions with the formation of side products as lithium carbonate, lithium formate, lithium acetate, CO_2 , and H_2O , which will further form Li_2CO_3 and LiOH . The Li_2O_2 may come from the disproportionation reaction ($2\text{LiO}_2 \rightarrow 2\text{Li}_2\text{O}_2 + \text{O}_2$) and/or the further electrochemical reaction ($\text{LiO}_2 + \text{Li}^+ + \text{e}^- \rightarrow \text{Li}_2\text{O}_2$) of LiO_2 . For simplicity, the formation kinetics of Li_2O_2 is expressed according to Reaction I as:

$$j_I = nF \left\{ k_{Ia} (c_{Li_2O_2,s}) \exp \left[\frac{(1-\beta)nF}{RT} \eta_I \right] - k_{Ic} (c_{Li^+,s})^2 (c_{O_2,s}) \exp \left(\frac{-\beta nF}{RT} \eta_I \right) \right\} \quad (21)$$

where k_{Ia} and k_{Ic} are the anodic and cathodic rate constant, respectively. η_I is the overpotential of Reaction I at the cathode. The degradation of solvent can be described based on Sahapatsombut's work as [27]:

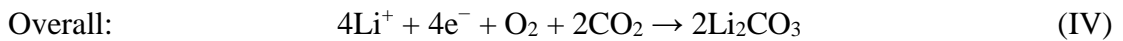
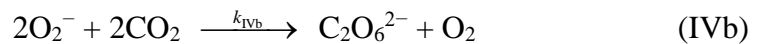


Through taking the solvent concentration as constant, the kinetic is expressed using the Tafel form rather than the Butler-Volmer form as the large kinetic overpotential during discharge puts the reaction in the Tafel region and considers the irreversible for electrolyte degradation:

$$j_{III} = Fk_{III}(c_{O_2,s}) \left[-\exp \left(\frac{-\beta nF}{RT} \eta_{III} \right) \right] \quad (22)$$

where k_{III} and η_{III} are the corresponding rate constant and overpotential, respectively.

After that, CO_2 and H_2O will further participate in the electrochemical and/or chemical reactions. Here, one possible mechanism for the electrochemical formation of Li_2CO_3 is taken as an example:

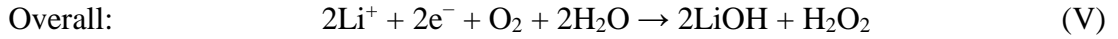
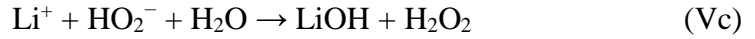
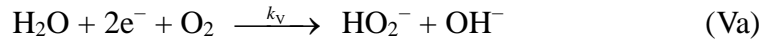


The reaction kinetics can be expressed:

$$j_{IVa} = Fk_{IVa}(c_{O_2,s}) \left[-\exp\left(\frac{-\beta nF}{RT}\eta_{IV}\right) \right] \quad (23a)$$

$$r_{IVb} = k_{IVb}(c_{O_2,s})(c_{CO_2,s}) \quad (23b)$$

where k_{IVa} and k_{IVb} are the rate constants for the electrochemical reaction to form O_2^- and chemical reaction to generate Li_2CO_3 , respectively. η_{IV} is the overpotential for the reaction. The continuous reactions IVa and IVb describe the irreversible reduction of CO_2 and thus a Tafel form is used in Eq. 23a. It has been demonstrated that the Reaction IVb is first-order and is the rate determining step, so that the other reaction is considered as equilibrium. Similarly, one possible mechanism for the electrochemical formation of $LiOH$ is [59]:



The reaction kinetics is expressed as:

$$j_v = nFk_v(c_{H_2O,s})(c_{O_2,s}) \left[-\exp\left(\frac{-\beta nF}{RT}\eta_v\right) \right] \quad (24)$$

where k_v is the rate constant and η_{IV} is the corresponding overpotential. The other reactions considered as equilibrium.

As all reactions occurred during discharge, the conservation of current in Eq. 7 becomes:

$$\nabla \cdot \mathbf{i}_l = \sum_m a j_m \quad (25)$$

where m stands for individual reactions from Reaction I to V. Eq. 25 also includes the formation of side products (Li_2O_2 , Li_2CO_3 , LiOH) and the decomposition of the solvent. In addition, the volume fraction of the solid discharge products (LiO_2 , Li_2O_2 , Li_2CO_3 , and LiOH) is expressed by the following equation instead of Eq. 15 as:

$$\frac{\partial \varepsilon_s}{\partial t} = \sum_{\text{solid phase } m} a j_m \frac{M_m}{nF \rho_m} \quad (26)$$

The inclusion of Eqs. 21-26 may help to build up a more comprehensive model for LiO_2 -based batteries with side reactions. However, due to the unknown reaction kinetics and the absence of detailed side product ratios [22], a numerical validation is hard at the present stage. In the future work, more efforts are needed in unrevealing the reaction mechanisms (e.g., Reaction IV and V) and measuring the related parameters (e.g., reaction rate constant, ratio of side products) for a better combination of experimental and modeling works.

4.2 Charge process

The modeling works focusing on the charge process of Li-O_2 batteries have few been reported [24], which may be attributed to the unclear decomposition mechanisms of Li_2O_2 [60]. Different from the case in Li_2O_2 -based batteries, in LiO_2 -based batteries the main electrochemical reaction is Reaction II, which seems to be a one-step reaction without different routes. Based on this reaction, if the charge process is a reversed electrochemical one, as illustrated in **Fig. 9**, the electron transport resistance should decrease with the charge process, resulting in a voltage curve that keeps decreasing till the end of charge. However, on the contrary, the charge voltage of the LiO_2 -based battery kept increasing during charge in each cycle (**Fig. S5a**). From the

detailed characterization of the product, the results demonstrated that the LiO_2 is stable enough for repeated cycles with few generated side products [22]. Consequently, the irreversible side reactions as described in Section 4.1 would hardly lead to the increased voltage during charge. After the failure of the battery, it is found that the lithium anode was converted to LiOH due to the oxygen crossover (**Fig. S5b**). Thus, the increased resistance for lithium ion deposition might be the main reason for the shape of the charge curve and the performance degradation. This result indicates that to model the charge process, only considering the reaction occur at the cathode may be not enough. A comprehensive model with taking the whole battery into consideration is in great need.



Fig. 9 Schematically shown of the possible route of the LiO_2 decomposition: (a) The thickness of the film-like product decreases; (b) The volume of the product shrinks. In both cases, the electronic resistance should decrease with the charge process.

5. Conclusions

In this work, we have conducted a numerical investigation of the discharge behaviors of a non-aqueous Li-O_2 battery based on LiO_2 as the product. A mathematical model with macroscopic continuum approach was first developed and validated with experimental results. Based on this model, the effects of electrode and electrolyte properties on the discharge performance were detailedly investigated. Key conclusions are listed as follows:

- (1) For the cathode geometry, a thin cathode can facilitate oxygen transport and is favorable for a higher specific capacity (mAh g^{-1}), but a thick cathode may deliver a higher practical capacity (mAh) at the same current density. A large porosity is crucial for both species transport and solid product accumulation, and thus is the key to delivering a high specific capacity.
- (2) For the cathode activity, under the condition of the film-like LiO_2 morphology, an increase in the activities leads to an apparent increase in the discharge voltage but unobvious changes in the discharge capacity.
- (3) The oxygen solubility and diffusivity have similar impacts on discharge capacities, but the oxygen solubility has a larger impact on energy densities.

Besides numerical investigations of the cathode and electrolyte properties, the limitations and further developments of the present model are also discussed:

- (1) Even for a cathode with the same porosity, the pore size distribution may be different and should be considered.
- (2) The morphology of the solid product may change with the catalytic activity, and thus an in-depth understanding in the LiO_2 morphology evolution process is needed.
- (3) The oxygen solubility and diffusivity may be correlated and change with the lithium salt concentration. In addition, lithium ion diffusion may also become the limiting factor when an electrolyte with low salt concentrations is used and should also be carefully addressed.
- (4) The effects of side reactions, including the formation of Li_2O_2 and the

decomposition of the electrolyte, should be included in the model for an insightful investigation.

- (5) When describing the charge process, a comprehensive model that takes the reactions occurred at both the cathode and the lithium anode into account is in great demand.

This work can be potentially used to optimize the electrode and electrolyte for this newly developed LiO₂-based batteries, and provide implications for other energy storage systems with solid product formation such as Na-O₂ batteries and Li-S batteries.

Acknowledgment

M. NI thanks the funding support from The Hong Kong Polytechnic University (G-YBJN and G-YW2D), the Environment Conservation Fund (ECF 54/2015) and a fund from RISUD (1-ZVEA).

Nomenclature

<i>a</i>	active surface area per unit electrode volume ($\text{m}^2 \text{m}^{-3}$)
<i>c</i>	concentration (mol m^{-3})
<i>D</i>	diffusion coefficient ($\text{m}^2 \text{s}^{-1}$)
<i>d</i>	distance (m)
<i>E</i>	potential (V)
<i>F</i>	Faraday constant ($96,485 \text{ C mol}^{-1}$)
<i>i</i>	current density (A m^{-2})
<i>j</i>	local transfer current density (A m^{-2})
<i>k</i>	rate constant
<i>L</i>	length (m)
<i>M</i>	molecular weight (g mol^{-1})
<i>n</i>	number of electrons transferred in the electrode reaction
<i>N</i>	molar flux
<i>R</i>	universal gas constant ($8.314 \text{ J mol}^{-1} \text{K}^{-1}$)
<i>S</i>	reaction rate ($\text{mol m}^{-3} \text{s}^{-1}$)

s	stoichiometric coefficient
T	temperature (K)
t_+	transference number of cation

Greek

α	Bruggeman coefficient
β	symmetry factor
δ	thickness (m)
ε	porosity or volume fraction
η	overpotential (V)
κ	ionic conductivity (S m^{-1})
ρ	density (kg m^{-3})
σ	electrical conductivity (S m^{-1})
ϕ	electric potential (V)

Superscripts and subscripts

0	equilibrium or initial value
app	applied value
a	anode
c	cathode
eff	effective value
l	liquid phase
s	solid phase; solid product

References

- [1] Wagner FT, Lakshmanan B, Mathias MF. Electrochemistry and the Future of the Automobile. *J Phys Chem Lett* 2010;1:2204-19.
- [2] Tan P, Wei Z, Shyy W, Zhao TS. Prediction of the theoretical capacity of non-aqueous lithium-air batteries. *Appl Energy* 2013;109:275-82.
- [3] Viswanathan V, Thygesen KS, Hummelshøj JS, Nørskov JK, Girishkumar G, McCloskey BD et al. Electrical conductivity in Li_2O_2 and its role in determining capacity limitations in non-aqueous Li- O_2 batteries. *J Chem Phys* 2011;135:214704.
- [4] Tan P, Shyy W, Wei ZH, An L, Zhao TS. A carbon powder-nanotube composite cathode for non-aqueous lithium-air batteries. *Electrochim Acta* 2014;147:1-8.

- [5] Lu Y, Gallant BM, Kwabi DG, Harding JR, Mitchell RR, Whittingham MS et al. Lithium-oxygen batteries: bridging mechanistic understanding and battery performance. *Energy Environ Sci* 2013;6:750-68.
- [6] Ottakam Thotiyil MM, Freunberger SA, Peng Z, Bruce PG. The carbon electrode in nonaqueous Li-O₂ cells. *J Am Chem Soc* 2013;135:494-500.
- [7] Feng N, He P, Zhou H. Critical challenges in rechargeable aprotic Li-O₂ batteries. *Adv Energy Mater* 2016;6:1502303.
- [8] Guo Z, Zhou D, Liu H, Dong X, Yuan S, Yu A et al. Synthesis of ruthenium oxide coated ordered mesoporous carbon nanofiber arrays as a catalyst for lithium oxygen battery. *J Power Sources* 2015;276:181-8.
- [9] Tan P, Shyy W, Zhao T, Zhang R, Zhu X. Effects of moist air on the cycling performance of non-aqueous lithium-air batteries. *Appl Energy* 2016;182:569-75.
- [10] Jian Z, Liu P, Li F, He P, Guo X, Chen M et al. Core-Shell-Structured CNT@RuO₂ composite as a high-performance cathode catalyst for rechargeable Li-O₂ Batteries. *Angewandte Chemie-International Edition* 2014;53:442-6.
- [11] Chen Y, Freunberger SA, Peng Z, Fontaine O, Bruce PG. Charging a Li-O₂ battery using a redox mediator. *Nat Chem* 2013;5:489-94.
- [12] Bergner BJ, Schurmann A, Peppler K, Garsuch A, Janek J. TEMPO: A mobile catalyst for rechargeable Li-O₂ batteries. *J Am Chem Soc* 2014;136:15054-64.
- [13] Lim H, Song H, Kim J, Gwon H, Bae Y, Park K et al. Superior rechargeability and efficiency of lithium-oxygen batteries: Hierarchical air electrode architecture combined with a soluble catalyst. *Angew Chem Int Edit* 2014;53:3926-31.

- [14] Peng Z, Freunberger SA, Hardwick LJ, Chen Y, Giordani V, Barde F et al. Oxygen reactions in a non-aqueous Li^+ electrolyte. *Angew Chem Int Edit* 2011;50:6351-5.
- [15] Yang J, Zhai D, Wang H, Lau KC, Schlueter JA, Du P et al. Evidence for lithium superoxide-like species in the discharge product of a Li-O₂ battery. *Phys Chem Chem Phys* 2013;15:3764-71.
- [16] Zhai D, Wang H, Yang J, Lau KC, Li K, Amine K et al. Disproportionation in Li-O₂ batteries based on a large surface area carbon cathode. *J Am Chem Soc* 2013;135:15364-72.
- [17] Xia C, Waletzko M, Chen L, Peppler K, Klar PJ, Janek J. Evolution of Li₂O₂ growth and its effect on kinetics of Li-O₂ batteries. *ACS Appl Mater Interfaces* 2014;6:12083-92.
- [18] Lee B, Kim J, Yoon G, Lim H, Choi I, Kang K. Theoretical evidence for low charging overpotentials of superoxide discharge products in metal–oxygen batteries. *Chem Mater* 2015;27:8406-13.
- [19] Zhai D, Lau KC, Wang H, Wen J, Miller DJ, Kang F et al. The effect of potassium impurities deliberately introduced into activated carbon cathodes on the performance of lithium–oxygen batteries. *ChemSusChem* 2015;8:4235-41.
- [20] Fan W, Wang B, Guo X, Kong X, Liu J. Nanosize stabilized Li-deficient Li_{2-x}O₂ through cathode architecture for high performance Li-O₂ batteries. *Nano Energy* 2016;27:577-86.

- [21] Yang Y, Zhang T, Wang X, Chen L, Wu N, Liu W et al. Tuning the morphology and crystal structure of Li_2O_2 : A graphene model electrode study for Li– O_2 battery. *ACS Appl Mater Interfaces* 2016;8:21350-7.
- [22] Lu J, Lee YJ, Luo X, Lau KC, Asadi M, Wang H et al. A lithium-oxygen battery based on lithium superoxide. *Nature* 2016;529:377-83.
- [23] Franco AA, Xue K. Carbon-based electrodes for lithium air batteries: scientific and technological challenges from a modeling perspective. *ECS Journal of Solid State Science and Technology* 2013;2:M3084-100.
- [24] Yuan J, Yu J, Sundén B. Review on mechanisms and continuum models of multi-phase transport phenomena in porous structures of non-aqueous Li-Air batteries. *J Power Sources* 2015;278:352-69.
- [25] Li X, Faghri A. Optimization of the cathode structure of lithium-air batteries based on a two-dimensional, transient, non-isothermal model. *J Electrochem Soc* 2012;159:A1747-54.
- [26] Tan P, Shyy W, An L, Wei ZH, Zhao TS. A gradient porous cathode for non-aqueous lithium-air batteries leading to a high capacity. *Electrochem Commun* 2014;46:111-4.
- [27] Sahapatsombut U, Cheng H, Scott K. Modelling of electrolyte degradation and cycling behaviour in a lithium–air battery. *J Power Sources* 2013;243:409-18.
- [28] Cheng H, Scott K. Selection of oxygen reduction catalysts for rechargeable lithium-air batteries-Metal or oxide? *Applied Catalysis B-Environmental* 2011;108:140-51.

- [29] Sahapatsombut U, Cheng H, Scott K. Modelling the micro–macro homogeneous cycling behaviour of a lithium–air battery. *J Power Sources* 2013;227:243-53.
- [30] Gwak G, Ju H. Three-dimensional transient modeling of a non-aqueous electrolyte lithium-air battery. *Electrochim Acta* 2016;201:395-409.
- [31] Yoo K, Banerjee S, Dutta P. Modeling of volume change phenomena in a Li–air battery. *J Power Sources* 2014;258:340-50.
- [32] Huang J, Faghri A. Analysis of electrolyte level change in a lithium air battery. *J Power Sources* 2016;307:45-55.
- [33] Huang J, Faghri A. Capacity enhancement of a lithium oxygen flow battery. *Electrochim Acta* 2015;174:908-18.
- [34] Wang Y, Wang Z, Yuan H, Li T. Discharge oxide storage capacity and voltage loss in li-air battery. *Electrochim Acta* 2015;180:382-93.
- [35] Sandhu SS, Brutchen GW, Fellner JP. Lithium/air cell: Preliminary mathematical formulation and analysis. *J Power Sources* 2007;170:196-209.
- [36] Li X, Huang J, Faghri A. A critical review of macroscopic modeling studies on Li O₂ and Li–air batteries using organic electrolyte: Challenges and opportunities. *J Power Sources* 2016;332:420-46.
- [37] Adams BD, Black R, Radtke C, Williams Z, Mehdi BL, Browning ND et al. The Importance of Nanometric Passivating Films on Cathodes for Li-Air Batteries. *ACS Nano* 2014;8:12483-93.

- [38] Cui Z, Guo X, Li H. Equilibrium voltage and overpotential variation of nonaqueous Li–O₂ batteries using the galvanostatic intermittent titration technique. *Energy Environ Sci* 2015;8:182-7.
- [39] Padbury R, Zhang X. Lithium–oxygen batteries—Limiting factors that affect performance. *J Power Sources* 2011;196:4436-44.
- [40] Zhang J, Wang D, Xu W, Xiao J, Williford RE. Ambient operation of Li/Air batteries. *J Power Sources* 2010;195:4332-7.
- [41] Jung CY, Zhao TS, An L. Modeling of lithium–oxygen batteries with the discharge product treated as a discontinuous deposit layer. *J Power Sources* 2015;273:440-7.
- [42] Laoire CO, Mukerjee S, Abraham KM, Plichta EJ, Hendrickson MA. Influence of nonaqueous solvents on the electrochemistry of oxygen in the rechargeable lithium-air battery. *Journal of Physical Chemistry C* 2010;114:9178-86.
- [43] Nyman A, Behm M, Lindbergh G. Electrochemical characterisation and modelling of the mass transport phenomena in LiPF₆–EC–EMC electrolyte. *Electrochim Acta* 2008;53:6356-65.
- [44] Li X. A modeling study of the pore size evolution in lithium-oxygen battery electrodes. *J Electrochem Soc* 2015;162:A1636-45.
- [45] Amestoy PR, Duff IS, L'Excellent J, Koster J. MUMPS: A General Purpose Distributed Memory Sparse Solver. In: Sørøvik T, Manne F, Gebremedhin AH, Moe R. *Applied Parallel Computing. New Paradigms for HPC in Industry and Academia*:

5th International Workshop, PARA 2000 Bergen, Norway, June 18-20, 2000

Proceedings, Berlin, Heidelberg: Springer Berlin Heidelberg; 2001:121-130.

[46] Ascher UM, Petzold LR. Computer methods for ordinary differential equations and differential-algebraic equations. Philadelphia: Soc Ind Appl Math; 1998.

[47] Xue K, Nguyen T, Franco AA. Impact of the cathode microstructure on the discharge performance of lithium air batteries: a multiscale model. J Electrochem Soc 2014;161:E3028-35.

[48] Ding N, Chien SW, Hor TSA, Lum R, Zong Y, Liu Z. Influence of carbon pore size on the discharge capacity of Li-O₂ batteries. J Mater Chem A 2014;2:12433-41.

[49] Zhu X, Zhao T, Tan P, Wei Z, Wu M. A high-performance solid-state lithium-oxygen battery with a ceramic-carbon nanostructured electrode. Nano Energy 2016;26:565-76.

[50] Ma Z, Yuan X, Li L, Ma Z, Wilkinson DP, Zhang L et al. A review of cathode materials and structures for rechargeable lithium-air batteries. Energy Environ Sci 2015;8:2144-98.

[51] Yilmaz E, Yogi C, Yamanaka K, Ohta T, Byon HR. Promoting formation of noncrystalline Li₂O₂ in the Li-O₂ battery with RuO₂ nanoparticles. Nano Letters 2013;13:4679-84.

[52] Burke CM, Pande V, Khetan A, Viswanathan V, McCloskey BD. Enhancing electrochemical intermediate solvation through electrolyte anion selection to increase nonaqueous Li-O₂ battery capacity. Proc Natl Acad Sci USA 2015;112:9293-8.

- [53] Balaish M, Kraytsberg A, Ein-Eli Y. A critical review on lithium-air battery electrolytes. *Phys Chem Chem Phys* 2014;16:2801-22.
- [54] Johnson L, Li C, Liu Z, Chen Y, Freunberger SA, Ashok PC et al. The role of LiO_2 solubility in O_2 reduction in aprotic solvents and its consequences for Li- O_2 batteries. *Nat Chem* 2014;6:1091-9.
- [55] Abraham KM. Electrolyte-directed reactions of the oxygen electrode in lithium-air batteries. *J Electrochem Soc* 2015;162:A3021-31.
- [56] Sergeev AV, Chertovich AV, Itkis DM, Goodilin EA, Khokhlov AR. Effects of cathode and electrolyte properties on lithium–air battery performance: Computational study. *J Power Sources* 2015;279:707-12.
- [57] Gittleson FS, Jones RE, Ward DK, Foster ME. Oxygen solubility and transport in Li–air battery electrolytes: establishing criteria and strategies for electrolyte design. *Energy Environ Sci* 2017;DOI:10.1039/C6EE02915A.
- [58] Das SK, Xu S, Emwas A, Lu YY, Srivastava S, Archer LA. High energy lithium-oxygen batteries-transport barriers and thermodynamics. *Energy Environ Sci* 2012;5:8927-31.
- [59] Wu S, Tang J, Li F, Liu X, Yamauchi Y, Ishida M et al. A synergistic system for lithium–oxygen batteries in humid atmosphere integrating a composite cathode and a hydrophobic ionic liquid-based electrolyte. *Adv Funct Mater* 2016;26:3691-8.
- [60] Tan P, Liu M, Shao Z, Ni M. Recent advances in perovskite oxides as electrode materials for nonaqueous lithium–oxygen batteries. *Adv Energy Mater* 2017; 1602674. DOI: 10.1002/aenm.201602674

Table captions

Table 1 Theoretical capacity of a non-aqueous Li-O₂ battery with different products

Table 2 Parameters used in simulation

Table 1 Theoretical capacity of a non-aqueous Li-O₂ battery with different products

Reaction	Theoretical specific based on the product (Ah kg ⁻¹)
$2\text{Li} + 0.5\text{O}_2 \rightarrow \text{Li}_2\text{O}$	1,794
$2\text{Li} + \text{O}_2 \rightarrow \text{Li}_2\text{O}_2$	1,168
$3\text{Li} + 2\text{O}_2 \rightarrow \text{Li}_3\text{O}_4$	948
$\text{Li} + \text{O}_2 \rightarrow \text{LiO}_2$	688

Table 2 Parameters used in simulation

Parameter	Symbol	Value	Unit	Ref.
Geometrical properties				
Thickness of the separator	L_{Sep}	5×10^{-5}	m	[40]
Thickness of the cathode	L_{Cat}	5×10^{-6}	m	
Porosity of the separator	ε_{Sep}	0.87	-	[29]
Porosity of the cathode	ε	0.94	-	
Conductivity of the cathode	σ	100	S m^{-1}	[41]
Distance between two graphene plat	d_0	2×10^{-8}	m	
Specific surface area of the cathode	a	9.4×10^7	$\text{m}^2 \text{m}^{-3}$	
Electrolyte properties				
Initial Li^+ concentration	c_{Li^+}	1000	mol m^{-3}	[22]
Initial O_2 concentration	c_{O_2}	4.427	mol m^{-3}	[42]
Solubility of LiO_2	c_{LiO_2}	1.0	mol m^{-3}	
Diffusion coefficient of Li^+	D_{Li^+}	8.98×10^{-10}	$\text{m}^2 \text{s}^{-1}$	[42]
Diffusion coefficient of O_2	D_{O_2}	2.17×10^{-10}	$\text{m}^2 \text{s}^{-1}$	[42]
Ionic conductivity of the electrolyte	κ	0.03	S m^{-1}	[42]
Transference number of Li^+	t_+	0.26	-	[43]
$\partial \ln f_{\pm} / \partial \ln c_{\text{Li}^+}$	-	-1.03	-	[43]
Kinetic parameter				
Exchange current at the anode	i_{a0}	1	A m^{-2}	[27]
Anodic rate constant	k_a	1.0×10^{-10}	m s^{-1}	
Cathodic rate constant	k_c	1.4×10^{-15}	$\text{m}^4 \text{mol}^{-1} \text{s}^{-1}$	
General parameter				
Electrical resistivity of LiO_2	R_s	1.0×10^8	Ωm	[18,44]
Density of LiO_2	ρ_{LiO_2}	2,180	kg m^{-3}	Assumed
Molecular weight of LiO_2	M_{LiO_2}	38.94	g mol^{-1}	
Density of reduced graphene oxide	ρ_{rGO}	2,260	kg m^{-3}	
Density of Ir	ρ_{Ir}	22,560	kg m^{-3}	
Operating temperature	T	298.15	K	

Figure captions

Fig. 1 Schematic diagram of a non-aqueous Li-O₂ battery during discharge. The inset demonstrates the reaction occurs inside the graphene-based cathode with the formation of LiO₂ as the product.

Fig. 2 Comparisons between simulated discharge curves and experimental data from Ref. [22]: (a) with a capacity limit of 1,000 mA h g⁻¹, the error bar shows the variation of discharge voltages during cycling; (b) deep discharge to a cut-off voltage of 2.2 V.

Fig. 3 Effect of cathode thickness on the discharge performance: (a) discharge voltage curves; (b) specific and practical capacities at different cathode thicknesses, the practical capacity is normalized using the capacity at the thickness of 5 μm; (c) oxygen concentration at the end of discharge; and (d) porosity profile at the end of discharge.

Fig. 4 Effect of cathode porosity on the discharge performance: (a) discharge voltage curves; (b) specific and practical capacities at different cathode thicknesses, the practical capacity is normalized using the capacity at the porosity of 0.94; (c) oxygen concentration at the end of discharge; and (d) normalized porosity profile at the end of discharge.

Fig. 5 Effect of reaction activity on the discharge performance: (a) discharge voltage curves; (b) average discharge voltages at different reaction rates.

Fig. 6 Effect of oxygen solubility on the battery with (a) pristine cathode (L=5 μm, ε₀=0.94), (b) thick cathode (L=20 μm, ε₀=0.94), and (c) compact cathode (L=5 μm, ε₀=0.76): (1) discharge voltage curves; (2) dimensionless oxygen concentration at the end of discharge; (3) normalized porosity profile at the end of discharge.

Fig. 7 Effect of oxygen diffusivity on the battery with (a) pristine cathode (L=5 μm, ε₀=0.94), (b) thick cathode (L=20 μm, ε₀=0.94), and (c) compact cathode (L=5 μm, ε₀=0.76): (1) discharge voltage curves; (2) dimensionless oxygen concentration at the end of discharge; (3) normalized porosity profile at the end of discharge.

Fig. 8 Comparison of normalized (a) specific capacity and (b) energy density of the battery at different ratios with: (1) pristine cathode; (2) thick cathode (large thickness); (3) compact cathode (low porosity).

Fig. 9 Schematically shown of the possible route of the LiO₂ decomposition: (a) The thickness of the film-like product decreases; (b) The volume of the product shrinks. In both cases, the electronic resistance should decrease with the charge process.